



Anthracene based organic dipolar compounds for sensitized solar cells

Yan-Zuo Lin ^a, Chiung Hui Huang ^a, Yuan Jay Chang ^{a,*}, Chia-Wei Yeh ^b, Tsung-Mei Chin ^c, Kai-Ming Chi ^b, Po-Ting Chou ^d, Motonori Watanabe ^e, Tahsin J. Chow ^{d,e,*}

^a Department of Chemistry, Tung Hai University, Taichung 40704, Taiwan

^b Department of Chemistry and Biochemistry, National Chung Cheng University, Chia-yi 621, Taiwan

^c Department of Applied Chemistry, Chinese Culture University, Taipei 111, Taiwan

^d Department of Chemistry, National Taiwan University, Taipei 106, Taiwan

^e Institute of Chemistry, Academia Sinica, Taipei 115, Taiwan

ARTICLE INFO

Article history:

Received 24 September 2013

Received in revised form 16 November 2013

Accepted 20 November 2013

Available online 27 November 2013

Keywords:

Dye-sensitized solar cells

Triarylene linked bridge

Anthracene based

Intramolecular charge transfer

ABSTRACT

Organic dyes that consist of an anthracene moiety between a triphenylamine donor group and a cyanoacrylic acid acceptor group displayed remarkable solar-to-energy conversion efficiency in dye-sensitized solar cells. The planar geometry of anthracene and its bulky substituents helped the dyes to form a high quality monolayer on the surface of TiO₂. A typical device made with the dye AN-Bu displayed a maximal photon-to-current conversion efficiency (IPCE) 65% in the region of 350–510 nm, a short-circuit photocurrent density (J_{sc}) 12.78 mA cm⁻², an open-circuit photovoltage (V_{oc}) 0.73 V, and a fill factor (FF) 0.67, corresponding to an overall conversion efficiency 6.23%. In an experiment of using deoxycholic acid (DCA) as a co-absorbent, the values of V_{oc} stayed in a similar range, yet the values of J_{sc} were reduced in ca. 11% due to a decrease of loading amounts. This result indicated that the quality of the dye films cannot be further improved by the adding of DCA. The photophysical properties were analyzed with the aid of a time-dependent density functional theory (TDDFT) model with the B3LYP functional.

© 2013 Elsevier Ltd. All rights reserved.

1. Introduction

In the design of organic dyes for sensitized solar cells (DSSCs), it has been established that a few key characters for an effective design of dye structures.^{1–4} One of them is the linear shape of molecules, which is usually a rigid rod with an electron donor (D) attached onto one terminal and an electron acceptor (A) onto the other side. During device fabrication, the dyes are absorbed on the surface of titanium oxide (TiO₂) forming a densely packed monolayer that acts as a p–n junction in the circuit. Upon photo-excitation, a charge transfer (CT) transition occurs from D to A along the long axis of the molecules. In a subsequent step the negative charge is injected inside TiO₂, while the positive charge is neutralized by the electrolyte. The morphology of the p–n junction, i.e., the organic monolayer, therefore plays a key factor for the performance of the solar cell.

The spacer group (S) of the dyes connecting D and A is usually a conjugated chromophore with considerable rigidity, so that the

dye molecules can stand vertically on the surface of TiO₂. The monolayer fabricated by the dye molecules has to cover the surface of TiO₂ as complete as possible to eliminate the presence of pinholes. A direct contact between TiO₂ and the electrolyte at the pinholes will lead to an unwanted charge recombination, therefore reduces the quantum efficiency. A typical way of achieving the maximal coverage is to add suitable substituents onto the dye structure, such as flexible long alkyl chains or bulky groups. However, the existence of bulky substituents may also repel each other on the surface of TiO₂, thus reduces the loading amount. An alternative way to achieve this goal is to enhance the ability of self-assembling of the dye molecules. A wide variety of organic dyes have been reported in the literature including the derivatives of coumarin,^{5,6} indoline,⁷ cyanine,^{8–12} perylene,^{13–17} dithiensirole,^{18,19} spirobifluorene,^{20–22} carbazole,^{23–27} and phenothiazine,^{28–35} etc. In this report we examine the possibility of using anthracene as part of the spacer group to enhance the morphology of the dyes.³⁶

The semiconducting properties of anthracene, tetracene, and pentacene derivatives have drawn considerable attention in the researches of organic opto-electronic materials. They have been successfully applied onto a variety of devices, such as organic field effect transistors, organic light emitting diodes, and organic

* Corresponding authors. Tel.: +886 4 23590248x305; fax: +886 4 23590426 (Y.J.C.); tel.: +886 2 27898552; fax: +886 2 27884179 (T.J.C.); e-mail addresses: jaychang@thu.edu.tw (Y.J. Chang), chowtj@gate.sinica.edu.tw (T.J. Chow).

photovoltaics. Among all acenes, anthracene possesses a size similar to the dihydrophenanthrene moiety in PA³⁷ and the phenothiazine in PNS (Fig. 1), while both have been reported to exhibit remarkable performance in DSSCs. In our previous studies, we have also shown that by locking the central double bond of stilbene in STR, the quantum efficiency of IND could be enhanced to a degree of ca. 15%.^{38,39} The planar shape and higher rigidity of the central ring system in these dyes is believed to have played a critical role in their DSSC performance.

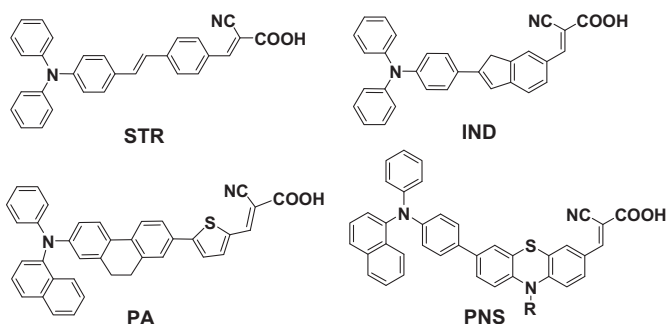


Fig. 1. Dye structures with proven DSSC performance.

2. Results and discussion

2.1. Synthesis strategies and chemical characterization

The structures of two dyes are shown in Fig. 2. An anthracene bridge moiety is placed between the amine donor moiety and the cyanoacrylic acid acceptor of the dyes. Either a triisopropylsilylithynyl or a butyl group is substituted at the 9,10-positions of anthracene. Their synthesis started from 2,6-diamino-anthraquinone as outline in Scheme 1. It was first converted to 2,6-dibromoanthraquinone, while the side groups of triisopropylsilylithynyl or butyl were introduced through a reductive procedure to form 2,6-dibromoanthracene for **3**.^{40,41} The bromine on one side of the anthracene was replaced by a triphenylamine through a Suzuki–Miyaura coupling reaction to produce **4** in 43–61% yield.⁴² The other bromine then was replaced by a thiophene-2-carbaldehyde unit through a Stille coupling reaction. The acetal protecting group was hydrolyzed to yield **6**.⁴³

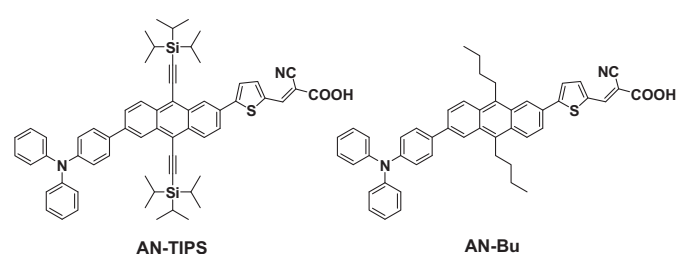


Fig. 2. Dye structures incorporating an anthracene unit in the center of backbone.

The formation of **AN-TIPS** and **AN-Bu** were completed by a Knoevenagel condensation with a cyanoacetic acid to build up the cyanoacrylic acid acceptor unit in yields of 61–70%.⁴⁴ All final products were crystallized into deep color solids, and were confirmed by their spectroscopic characteristics.

2.2. Photophysical properties

The absorption spectra of dyes in dilute THF solution (3×10^{-5} M) were shown in Fig. 3. They exhibit three major absorption regions appearing at 285–320 nm, 320–410 nm, and 410–550 nm. The first two regions were composed of localized aromatic $\pi-\pi^*$ transitions, and the last one was assigned to a charge-transfer (CT) transition. The CT band of **AN-TIPS** is slightly red-shifted with respect to that of **AN-Bu**, due to a π -conjugation with the TIPS substituents. The influence of π -conjugation can be shown by a comparison between **AN-TIPS** and **AN-Bu** using theoretical models, where the former exhibited a longer absorption wavelength yet a smaller extinction coefficient, i.e., $\epsilon = 1.75 \times 10^4 \text{ M}^{-1} \text{ cm}^{-1}$ and $2.50 \times 10^4 \text{ M}^{-1} \text{ cm}^{-1}$, respectively (Tables 1). These values are consistent with their oscillator strengths calculated by TDDFT, i.e., 0.36 and 0.45 (Table S1). In the $\pi-\pi^*$ transition region, both **AN-TIPS** and **AN-Bu** showed a high molar extinction coefficient ($> 4.00 \times 10^4 \text{ M}^{-1} \text{ cm}^{-1}$).

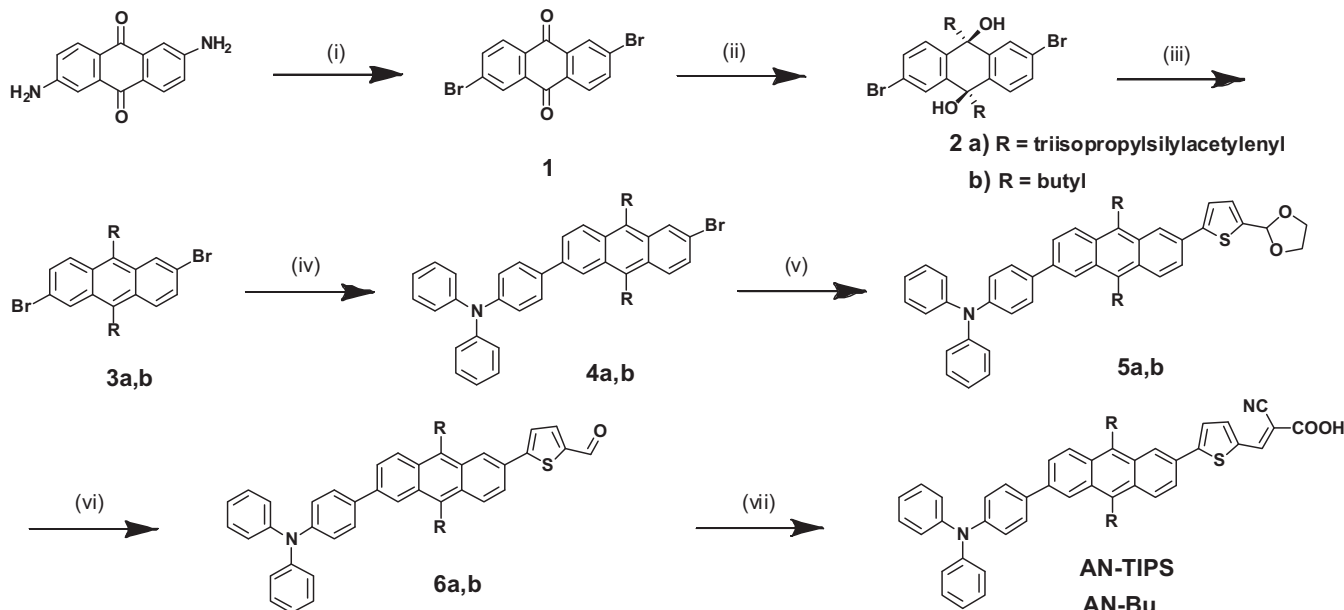
The dihedral angles between the planes of anthracene and the adjacent aminophenyl and thiophenyl rings were calculated to be ca. 32° and 23°, respectively (Fig. 4). The absorption spectra of dyes, after they were chemisorbed onto the surface of TiO₂, displayed a mild blue shift with respect to those in solutions (Fig. S10). Such a phenomenon has been observed previously, and was attributed to the reduction of electron accepting ability of the cyanoacrylate group comparing to a free carboxylic acid.^{45–47} The emission spectrum of **AN-Bu** showed a broader bandwidth with slightly large stoke shift, revealing a larger conformational re-adjustment upon photo-excitation (Fig. S11). A higher conformational flexibility can be beneficial to the device performance, as a better surface coverage may be achieved on top of TiO₂ that could retard the rate of charge recombination and therefore increase the photocurrent.

2.3. Electrochemical properties

The oxidation potentials (E_{ox}) were measured by cyclic voltammetry (CV) in THF, and the results were included in Table 1. The HOMO levels correspond to the first oxidation potentials (E_{ox}) of **AN-TIPS** and **AN-Bu**. The LUMO level was estimated by the values of E_{ox} and the zero-zero absorption wavelength, while the latter was obtained at the intersection of absorption and emission spectra. The HOMO–LUMO energy gap of **AN-TIPS** (2.31) was smaller than that of **AN-Bu** (2.43). The estimated LUMO levels of both dyes are sufficiently higher than the conductive band level of TiO₂ (ca. –0.5 V vs. NHE), while their HOMO levels are sufficiently lower than that of electrolyte ion pair I[–]/I₃[–] (ca. 0.4 V vs. NHE).^{48,49} It thus ensures an exothermic flow of charges through the photo-electronic conversion process (Fig. 5). The low level of HOMO (0.88 V) warrants an efficient charge regeneration after each light harvesting.

2.4. Theoretical calculation

The electronic configuration of the dyes was examined by using B3LYP/6-31G* hybrid functional implanted in a Q-Chem 3.0 software.⁵⁰ For the excited states, a time-dependent density functional theory (TDDFT) with the B3LYP functional was employed. The optimized molecular geometry of **AN-TIPS** and **AN-Bu** is shown in Fig. 4. The frontier orbital plots of HOMO and LUMO were drawn by using GaussView 4.1. The HOMO/LUMO energy levels and the corresponding band gaps are listed in Fig. 5 and Table 1 (also shown in Table S1 and Fig. S13). The parameters were found to be remarkably consistent with the experimental values. The electron density of HOMO is localized mainly on the amine moiety, while the LUMO at the cyanoacrylic acid (Fig. S13). In both the ground and excited states, the distribution of electron density is heavily coupled with



Scheme 1. Synthesis route of AN-series organic dyes. (i) CuBr_2 , $t\text{-BuONO}$, ACN, 90–100 °C; (ii) $n\text{-BuLi}$, triisopropylsilyl acetylene, THF, -78 °C; (iii) $\text{SnCl}_2\cdot 2\text{H}_2\text{O}$, AcOH , THF/ H_2O , rt; (iv) $\text{Pd}(\text{PPh}_3)_4$, 4-(diphenylamino)phenylboronic acid, K_2CO_3 (2 M), THF/toluene (1/2), 60 °C; (v) $\text{PdCl}_2(\text{PPh}_3)_2$, (5-(1,3-dioxolan-2-yl)thiophen-2-yl)tributylstannane, DMF, 90 °C; (vi) $\text{AcOH}/\text{THF}/\text{H}_2\text{O}$ (4/2/1), 60 °C; (vii) cyanoacetic acid, NH_4OAc , AcOH , 90–100 °C.

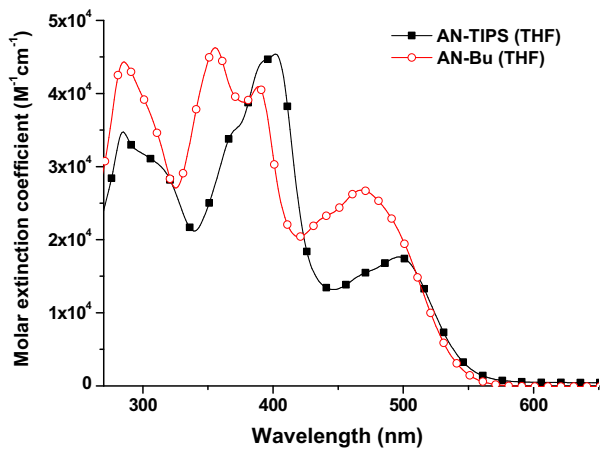


Fig. 3. Absorption spectra of the dyes in THF.

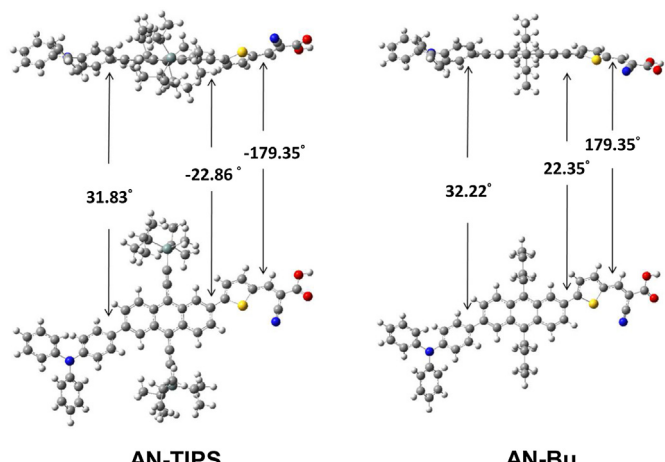


Fig. 4. Optimized molecular structure of the dyes.

Table 1

Calculated and experimental parameters of all dyes

Dye	HOMO/LUMO ^a (eV)	Band gap ^a	f^{b} (S1)	$\lambda_{\text{abs}}^{\text{c}}$ nm ($\text{e/M}^{-1} \text{cm}^{-1}$)	λ_{abs} nm (film)	$\lambda_{\text{em}}^{\text{b}}$ nm ($\text{e/M}^{-1} \text{cm}^{-1}$)	HOMO/LUMO ^d (eV)	E_{ox}^{e} (V)	E_{0-0}^{f} (V)	$E_{\text{red}}^{\text{g}}$ (V)
AN-TIPS	-4.99/-2.78	2.21	0.3580	500 (17,500)	492	611	-5.38/-3.07	0.88	2.31	-1.43
AN-Bu	-4.97/-2.67	2.30	0.4538	475 (25,000)	469	595	-5.38/-2.95	0.88	2.43	-1.55

^a: oscillator strength for the lowest energy transition; ^b: absorption coefficient; ^c: oxidation potential; ^d: LUMO calculated by HOMO+ E_{0-0} .
^e: E_{ox} calculated by HOMO+4.5 (eV) (vs NHE).
^f: E_{0-0} determined from the intersection of absorption and emission in THF.
^g: E_{red} calculated by $E_{\text{ox}}-E_{0-0}$.

^a TDDFT/B3LYP calculated values.

^b Absorptions and emission were measured in THF.

^c Oxidation potentials of dyes (10^{-3} M) in THF containing 0.1 M ($n\text{-C}_4\text{H}_9\text{)}_4\text{NPF}_6$ with a scan rate of 50 mV s⁻¹ (vs. Fc^+/Fc).

^d LUMO calculated by HOMO+ E_{0-0} .

^e E_{ox} calculated by HOMO+4.5 (eV) (vs NHE).

^f E_{0-0} determined from the intersection of absorption and emission in THF.

^g E_{red} calculated by $E_{\text{ox}}-E_{0-0}$.

the orbitals in the central bridge linkage. The anthracene moiety therefore functions as an effective charge carrier between D and A.

The difference in Mulliken charge shift surrounding D, B, and A segments, before (S_0 state) and after (S_1 state) the photo-excitation,

can be clearly depicted by the magnitude of bar charts (Fig. S12). Comparing with AN-TIPS, compound AN-Bu exhibits a better charge separation for more efficient electron injection. The presence of triisopropylsilyl ethynyl substituents in AN-TIPS can

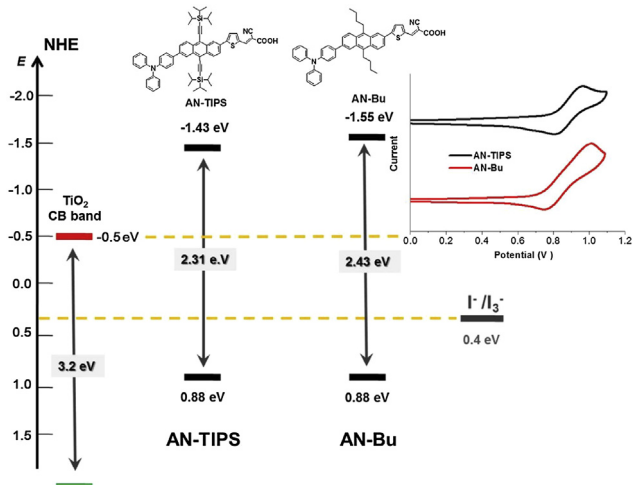


Fig. 5. Energy levels of HOMO and LUMO of dyes.

stabilize both the HOMO and LUMO levels (Fig. S13). It promotes the electron donating tendency of the triphenylamine donor, yet reduced the degree of charge separation in the excited state.

2.5. DSSCs performance

The DSSCs devices made with these two dyes were fabricated according to a standard procedure. The parameters were measured under AM 1.5 solar light (100 mW cm^{-2}), i.e., short-circuit current (J_{sc}), open-circuit photovoltage (V_{oc}), fill factor (FF), and solar-to-electrical photocurrent density (η) are summarized in Table 2. The photocurrent–voltage ($J-V$) plots of all devices are shown in Fig. 6. Two kinds of electrolytes were used in order to achieve the best result, i.e., system E1 was made of LiI (0.5 M), I₂ (0.05 M), and TBP (4-*tert*-butylpyridine) (0.5 M) in MeCN, and system E2 was composed of 3-dimethylimidazolium iodide (DMII)(1.0 M) and guanidinium thiocyanate (0.1 M), in addition to LiI (0.05 M), I₂ (0.03 M), and TBP (0.5 M) in a mixed solvent of MeCN and valeronitrile (85:15, v/v). An apparent improvement of V_{oc} values were observed by using the new type electrolyte E2, e.g., an increase of ca. 0.05–0.07 V was obtained with respect to those using E1 (Table 2). The relative quantum efficiency of **AN-Bu** was higher than that of **AN-TIPS**, a result attributed to the higher efficiency of electron injection to the conduction band of TiO₂. The devices made with **AN-Bu** and electrolyte E2 performed quite good, with J_{sc} 12.78 mA cm⁻², V_{oc} 0.73 V, and FF 0.67, which summed up to an overall quantum efficiency 6.23%. The incident photon-to-current conversion efficiency (IPCE) plots of the dyes are shown in Fig. 7.

Table 2
Photovoltaic parameters of devices under AM 1.5

Dye	E1/E2 ^a	J_{sc} (mA cm ⁻²)	V_{oc} (V)	FF	η^b (%)	Dye loading (10 ⁻⁷ mol/cm ²)
AN-TIPS	E1	11.99	0.67	0.63	5.06	2.48
	E2	11.61	0.72	0.65	5.42	
AN-Bu	E1	13.33	0.66	0.64	5.60	4.53
	E2	12.78	0.73	0.67	6.23	
N719	E1	16.89	0.73	0.60	7.38	—
	E2	15.46	0.76	0.64	7.52	

J_{sc} : short-circuit photocurrent density; V_{oc} : open-circuit photovoltage; FF: fill factor; η : total power conversion efficiency.

^a Electrolyte 1 (E1): LiI (0.5 M), I₂ (0.05 M), and TBP (0.5 M) in MeCN. Electrolyte 2 (E2): 3-dimethylimidazolium iodide (1.0 M), LiI (0.05 M), I₂ (0.03 M), guanidinium thiocyanate (0.1 M), and TBP (0.5 M) in MeCN/valeronitrile (85:15, v/v).

^b Performance of DSSC measured in a 0.25 cm² working area on an FTO (8 Ω/square) substrate.

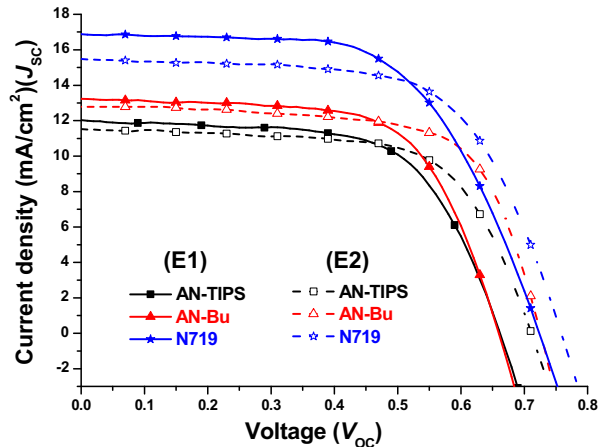
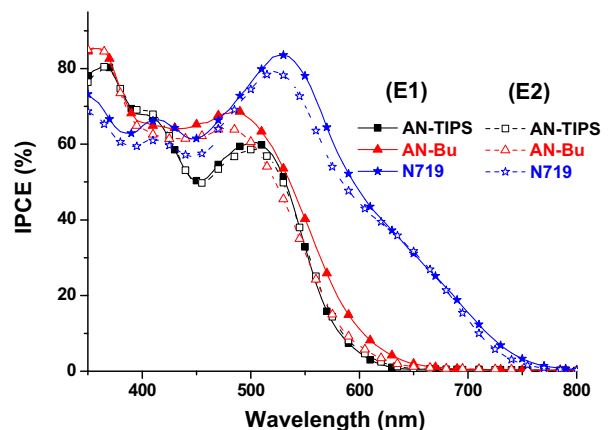
Fig. 6. $J-V$ curves of the dyes, with a comparison to N719.

Fig. 7. IPCE plots of the dyes, with a comparison with N719.

To further optimize the performance of DSSC, it is known that the alignment of dyes on the surface of TiO₂ is a critical factor. The organic compound needs to be planted vertically on the surface of metal oxide, and covers the surface as complete as possible. To avoid electrolyte contacting directly with TiO₂, the electrolyte was changed from E1 to E2. The lower concentration of LiI in E2 raised the conduction fermi level of TiO₂, therefore enhanced the V_{oc} value.^{51–53} The effect is supported by the higher resistance in the electrochemical impedance spectrum (EIS). The V_{oc} values of the devices using electrolyte E2 are considerably higher than those using electrolyte E1 (Table 2). The bulky side chains of both compounds also help preventing a contact between I₃ and the surface of TiO₂.²⁴ The size of **AN-TIPS** is larger than that of **AN-Bu**, therefore the former is able to reduce the dark current by decreasing the rate of charge recombination better than the latter.

Electrochemical impedance spectroscopic (EIS) analysis was performed to further elucidate the photovoltaic property.^{54,55} The EIS for the DSSCs made with these compounds were taken under a forward bias of –0.73 V in the dark. In the Nyquist plot (Fig. 8), a major semicircle was observed in a frequency range of 20–100 Hz, which is related to the transport process of injected electrons at the interfaces between TiO₂ and the electrolyte/dye.^{56–60}

The charge recombination resistance (R_{rec}) can be deduced by fitting the curves using a Z-view software.^{61,62} It is related to the charge recombination rate at the TiO₂ surface of DSSC, e.g., a larger R_{rec} indicates a slower charge recombination and therefore a larger V_{oc} values. The radius of the semicircle was enlarged along by using

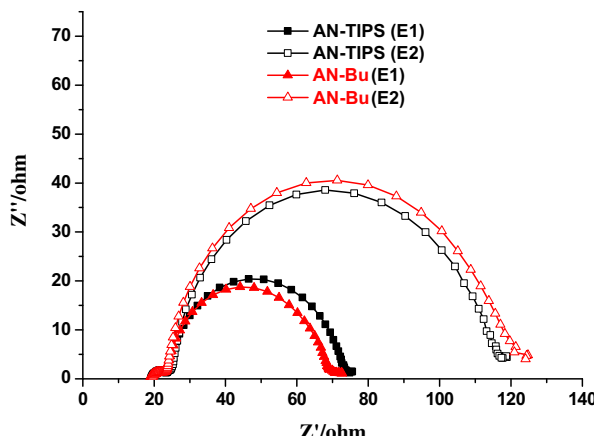


Fig. 8. EIS Nyquist plots of dyes at -0.73 V bias in the dark (i.e., minus imaginary part of the impedance $-Z''$ vs the real part of the impedance Z' when sweeping the frequency).

E2 electrolyte of Nyquist plot in the dark condition. This trend appears to be consistent with the V_{oc} values of AN-TIPS (E1, 0.67 V) \approx AN-Bu (E1, 0.66 V) $<$ AN-TIPS (E2, 0.72 V) \approx AN-Bu (E2, 0.73 V). In Bode phase plots, the peak position of middle-frequency is related to the electron lifetime, e.g., a shift to low-frequency corresponds to a longer electron lifetime. The injected electron lifetime (τ) can be estimated directly by fitting the plots into the equation of $\tau=1/(2\pi f)$, where f is the frequency. A larger value of V_{oc} corresponds to a longer electron lifetime, while the dyes that have quit high V_{oc} by using electrolyte E2 in these materials.

The effect of anthracene for improving the film morphology was examined by using deoxycholic acid (DCA). For some dyes that were not able to form high quality films, the addition of DCA as a co-absorbent can effectively improve the film morphology, and consequently reduce the rate of charge recombination.^{56,57,59,60} However, the addition of DCA may not improve the devices whose morphology are already of sufficient quality. Upon the addition of DCA as a co-absorbent (10 mM), the open-circuit voltage was found not to be changed in a significant amount (Table 3). This is a firm evidence supporting our initial assumption that the inclusion of an anthracene unit in the structure of dyes can enhance the self-assembling ability for forming a high quality film. The FF values also stayed nearly the same in the range of 0.63 – 0.64 . As it would be expected, the values of short-circuit current were reduced. The J_{sc} values were dropped from 11.99 to 10.66 mA cm^{-2} for AN-TIPS, and from 13.33 to 11.87 mA cm^{-2} for AN-Bu. An overall

reduction of quantum efficiency in 8.30 – 9.28% was observed (Fig. 9). The decrease of J_{sc} value can be readily explained by a lower amount of loading, because the surface of TiO_2 was partly occupied by DCA (Fig. S21). The new design of including an anthracene moiety in organic dyes does provide a profound effect of improving film morphology.

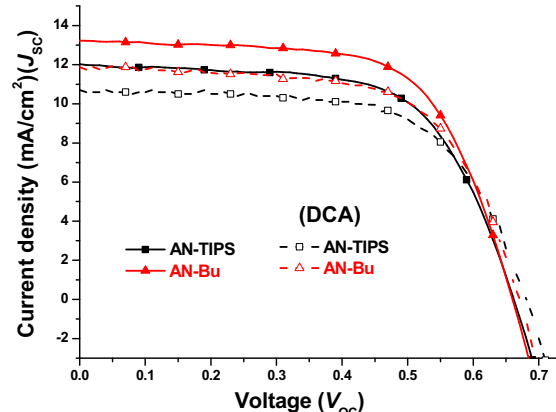


Fig. 9. J – V curves of dyes with different concentrations of DCA.

A comparison of our results with a few recent reports involving anthracene is instructive (Fig. 10). The remarkable performance of compound AN-26, prepared by Lin and Ho, reached the highest quantum efficiency of 9.11% in the presence of DCA (Table 3).⁶⁵ It took the advantage of high J_{sc} value induced by the 2,6-disubstituted anthracene unit. In another two reports of AN-910A³⁶ and AN-910B,⁶⁶ where the anthracene units were substituted at the 9 and 10 positions, the quantum efficiencies were reduced to 2 – 3% . The J_{sc} values were substantially reduced due to the lower degree of π -conjugation along the main chromophore. These results strongly implies that a 2,6-disubstituted anthracene can act a highly efficient spacer group, significantly better than the 9,10-disubstituted derivative, in the design of organic dyes for DSSCs.

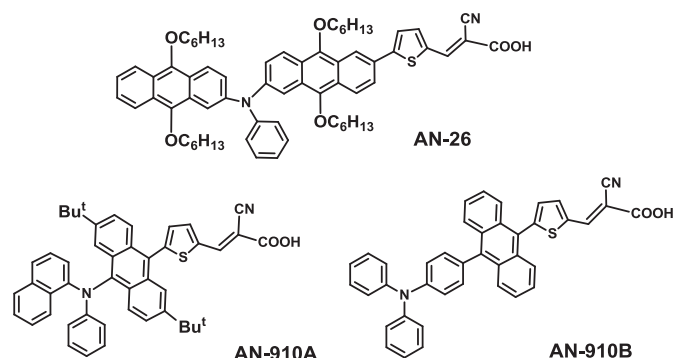


Fig. 10. Organic dyes containing anthracene chromophores.

3. Conclusion

The 2,6-disubstituted anthracene derivatives, AN-TIPS and AN-Bu, were proven to be effective dyes for the application on DSSCs. The planar shape of anthracene, along with the bulky TIPS and butyl substituents, exhibited a good film-forming property on the surface of TiO_2 . Both dyes displayed remarkable solar-to-energy conversion efficiency. A typical device made with AN-Bu dye performed a maximal photon-to-current conversion efficiency (IPCE) 65% in the region of 350 – 510 nm, a short-circuit photocurrent

Table 3
Photovoltaic parameters of devices made with and without DCA

Dye ^a	DCA (mM)	J_{sc} (mA cm^{-2})	V_{oc} (V)	FF	η^b (%)
AN-TIPS	0	11.99	0.67	0.63	5.06
	10	10.66	0.69	0.63	4.61
AN-Bu	0	13.33	0.66	0.64	5.60
	10	11.87	0.68	0.63	5.08
AN-26^c	0	16.63	0.71	0.64	7.52
	10	18.44	0.74	0.66	9.11
AN-910A^d	0	6.00	0.565	0.648	2.20
AN-910B^e	0	5.39	0.678	0.797	2.91

J_{sc} : short-circuit photocurrent density; V_{oc} : open-circuit photovoltage; FF: fill factor; η : total power conversion efficiency.

^a Concentration of dye is 3×10^{-4} M in THF.

^b Performance of DSSC measured in a 0.25 cm^2 working area on an FTO ($8 \Omega/\text{square}$) substrate with electrolyte 1 (E1) under AM 1.5 condition.

^c Ref. 65.

^d Ref. 36.

^e Ref. 66.

density (J_{sc}) 12.78 mA cm⁻², an open-circuit photovoltage (V_{oc}) 0.73 V, and a fill factor (FF) 0.67, corresponding to an overall conversion efficiency of 6.23%. The easy preparation of anthracene derivatives provides a handy entry for making useful dyes for solar cells.

4. Experimental section

4.1. General information

All reactions and manipulations were carried out under a nitrogen atmosphere. Solvents were distilled freshly according to standard procedures. ¹H and ¹³C NMR spectra were recorded on Bruker (AVIII 300/AV 400/AV 500 MHz) spectrometer in CDCl₃, THF-*d*₈, and DMSO-*d*₆ as a solvent. Chemical shifts are reported in scale down-field from the peak for tetramethylsilane. Absorption spectra were recorded on a Jasco-550 spectrophotometer. Emission spectra were obtained from a Hitachi F-4500 spectrofluorimeter. The emission spectra in solutions were measured in spectral grade solvent by a 90° angle detection. The redox potentials were measured by using cyclic voltammetry on CHI 620 analyser. The data were collected and analyzed using electrochemical analysis software. All measurements were carried out in THF solutions containing 0.1 M tetrabutylammonium hexafluorophosphate (TBAPF₆) as supporting electrolyte at ambient condition after purging 10 min with N₂. The conventional three electrode configuration was employed, which consists of a glassy carbon working electrode, a platinum counter electrode, and a Ag/AgNO₃ (0.1 M) reference electrode calibrated with ferrocene/ferrocenium (Fc/Fc⁺) as an internal reference with a scan rate of 50 V s⁻¹. Mass spectra were recorded on a VG70-250S mass spectrometer. The cell containing the solution of the sample (1 mM) and the supporting electrolyte was purged with nitrogen gas thoroughly before measurements. The oxidation potentials of organic dyes were estimated by averaging the anodic and cathodic peak potentials. The HOMO and LUMO values were calculated with reference to the ferrocene oxidation potential by using the following equations: HOMO = $E_{ox} + 4.8$ eV; LUMO = HOMO - E_{0-0} , where the HOMO of ferrocene was set at 4.8 eV.

The chemicals, i.e., 2,6-diaminoanthracene-9,10-dione, copper (II) bromide, *tert*-butyl nitrite (*t*-BuONO), triisopropylsilyl acetylene, tin(II) chloride dihydrate (SnCl₂·2H₂O), tetrakis(triphenyl phosphine)palladium (0) (Pd(PPh₃)₄), *n*-butyllithium (1.6 M in hexane), *trans*-dichlorobis (triphenylphosphine) palladium (II) (PdCl₂(PPh₃)₂), *N,N*-dimethylformamide, *N*-bromosuccinimide (NBS), tri-*n*-butyltin chloride, cyanoacetic acid, ammonium acetate, and acetic acid glacial, were purchased from ACROS, Alfa, Merck, Lancaster, TCI, Sigma-Aldrich, Showa, separately, and purified while necessary. Chromatographic separations were carried out by using silica gel from Merk, Kieselgel si 60 (40–63 µm). All structures were confirmed by their spectroscopic data were provided in *Supplementary data*.

4.1.1. 2,6-Dibromoanthracene-9,10-dione (1).⁶³ To a three-necked flask containing a mixture of 2,6-diaminoanthracene-9,10-dione (5 g, 21.0 mmol), CuBr₂ (11.72 g, 52.5 mmol), and *t*-BuONO (6.3 mL, 52.5 mmol) was added acetonitrile (250 mL). The reaction mixture was stirred at 90 °C for 24 h. After cooling, the mixture was quenched by adding 20% HCl, and filtered to give brown solid in 97% yield (7.5 g, 20.5 mmol); mp >300 °C; ¹H NMR (300 MHz, CDCl₃): δ 8.43 (s, 2H), 8.17 (d, 2H, *J*=8.4 Hz), 7.95 (d, 2H, *J*=8.4 Hz). ¹³C NMR (125 MHz, CDCl₃): δ 137.4, 130.4, 129.1; MS (EI, 70 eV): *m/z* (relative intensity) 363 (M⁺, 100); HRMS calcd for C₁₄H₆Br₂O₂: 363.8735, found 363.8744.

4.1.2. 2,6-Dibromo-9,10-bis(2-(triisopropylsilyl)ethynyl)anthracene (3a).⁶⁴ A mixture of triisopropylsilyl acetylene (TIPS) (6.7 mL,

29.9 mmol) in dry THF (20 mL) was placed in a three-necked flask under a nitrogen atmosphere, and to it was added n-BuLi (5 mL, 1.6 M in hexane) in an ice bath. After stirring at rt for 1 h, the mixture was transferred to another three-necked flask containing **1** (5 g, 13.7 mmol) in THF (50 mL) under -78 °C. After 12 h, the reaction was quenched by adding de-ionized water, followed by NH₄Cl_(aq). The mixture was extracted with ethyl acetate, and the organic layer was dried over anhydrous MgSO₄ and evaporated under vacuum. The crude mixture was added to a solution of SnCl₂·2H₂O (14 g, 62.0 mmol) and acetic acid (25 mL) in de-ionized water (25 mL). After 12 h, the reaction was quenched by adding de-ionized water and NaHCO_{3(aq)}. The mixture was extracted with ethyl acetate, and the organic layer was dried over anhydrous MgSO₄ and evaporated under vacuum. The product was purified by silica gel column chromatograph eluted with hexane. Yellow solid was obtained in 43% yield (4.1 g, 5.9 mmol). Mp 157–159 °C; ¹H NMR (300 MHz, CDCl₃): δ 8.80 (s, 2H), 8.45 (d, 2H, *J*=9.2 Hz), 7.66 (d, 2H, *J*=9.3 Hz), 1.25–1.28 (m, 42 H); ¹³C NMR (75 MHz, CDCl₃): δ 133.2, 130.9, 130.8, 129.5, 128.9, 122.0, 118.1, 106.3, 102.2, 18.8, 11.4. MS (EI, 70 eV): *m/z* (relative intensity) 695 ((M+H)⁺, 100); HRMS calcd for C₃₆H₄₉Br₂Si₂: 695.1740, found 695.1755.

4.1.3. 2,6-Dibromo-9,10-dibutylanthracene (3b). Compound **3b** was synthesized according to the same procedure as that of **3a**. Yellow solid of **3b** was obtained in 33% yield. Mp 101–103 °C; ¹H NMR (500 MHz, CDCl₃): δ 8.40 (s, 2H), 8.13 (d, 2H, *J*=9.5 Hz), 7.54 (dd, 2H, *J*=9.5, 1.5 Hz), 3.47 (t, 4H, *J*=8.0 Hz), 1.71–1.78 (m, 4H), 1.56–1.62 (m, 4H), 1.03 (t, 6H, *J*=7.5 Hz); ¹³C NMR (125 MHz, CDCl₃): δ 133.7, 130.5, 128.8, 128.3, 127.2, 127.1, 119.9, 33.5, 27.9, 23.2, 14.0. MS (EI, 70 eV): *m/z* (relative intensity) 446 (M⁺, 100); HRMS calcd for C₂₂H₂₄Br₂: 446.0245, found 446.0253.

4.1.4. *N*-(4-(2-Bromo-9,10-bis(2-(triisopropylsilyl)ethynyl)-anthracen-6-yl)phenyl)-*N*-phenylbenzenamine (4a). A mixture of **3a** (200 mg, 0.3 mmol), 4-(diphenylamino)phenylboronic acid (83 mg, 0.3 mmol), Pd(PPh₃)₄ (10.4 mg, 0.009 mmol) in 2 M K₂CO₃/THF/toluene at 90 °C in a three-necked flask under a nitrogen atmosphere. After 4 h, the reaction mixture was warmed up to room temperature and washed with brine. The mixture was extracted with CH₂Cl₂, then the organic layer was dried over anhydrous MgSO₄. Evaporation of the solvent gave a crude product, which was purified by silica gel column chromatograph eluted by CH₂Cl₂/hexane (1/9). Yellow solid of **4a** was obtained in 61% yield (157.4 mg, 0.18 mmol); mp 141–143 °C; ¹H NMR (400 MHz, CDCl₃): δ 8.81–8.82 (m, 2H), 8.61 (d, 1H, *J*=8.9 Hz), 8.46 (d, 1H, *J*=9.1 Hz), 7.90 (dd, 1H, *J*=9.1, 1.6 Hz), 7.68 (d, 2H, *J*=8.7 Hz), 7.63 (dd, 1H, *J*=9.0, 1.9 Hz), 7.29 (t, 4H, *J*=7.8 Hz), 7.16–7.19 (m, 6H), 7.05 (t, 2H, *J*=7.2 Hz), 1.2–1.3 (m, 42H); ¹³C NMR (100 MHz, CDCl₃): δ 147.5, 138.8, 134.0, 133.0, 132.8, 131.8131.0, 130.3, 139.4, 139.3, 129.1, 128.9, 128.0, 127.8, 126.9, 124.5, 124.1, 123.9, 123.7, 123.1, 122.6, 121.3, 118.8, 117.6, 105.6, 105.4, 102.9, 102.7, 18.9, 18.8, 11.5. MS (FAB, 70 eV): *m/z* (relative intensity) 860 ((M+H)⁺, 100); HRMS calcd for C₅₄H₆₃BrNSi₂: 860.3682, found 860.3704.

4.1.5. *N*-(4-(2-Bromo-9,10-dibutylanthracen-6-yl)phenyl)-*N*-phenylbenzenamine (4b). Compound **4b** was synthesized according to the same procedure as that of **4a**. Yellow solid of **4b** was obtained in 43% yield; mp 124–126 °C; ¹H NMR (400 MHz, CDCl₃): δ 8.43 (s, 1H), 8.42 (s, 1H), 8.33 (d, 1H, *J*=9.2 Hz), 8.16 (d, 1H, *J*=9.4 Hz), 7.78 (d, 1H, *J*=10.0 Hz), 7.66 (d, 2H, *J*=8.4 Hz), 7.52 (dd, 1H, *J*=1.5, 1.7 Hz), 7.29 (t, 4H, *J*=7.8 Hz), 7.21 (d, 2H, *J*=8.6 Hz), 7.19 (s, 2H), 7.17 (s, 2H), 7.06 (t, 2H, *J*=7.2 Hz), 3.60 (t, 2H, *J*=8.0 Hz), 3.52 (t, 2H, *J*=8.0 Hz), 1.76–1.81 (m, 4H), 1.59–1.66 (m, 4H), 1.01–1.07 (m, 7H), 0.83–0.89 (m, 3H); ¹³C NMR (100 MHz, CDCl₃): δ 147.6, 147.4, 136.8, 134.8, 134.4, 133.0, 130.3, 129.8, 129.3, 129.0, 128.2, 128.0, 127.9, 127.2, 125.8, 125.2, 124.6, 123.7, 123.1, 121.9, 119.3, 33.6, 33.5, 29.7, 27.9,

27.8, 23.3, 14.1, 14.0. MS (EI, 70 eV): m/z (relative intensity) 611 (M^+ , 100); HRMS calcd for $C_{40}H_{38}NBr$: 611.2188, found 611.2188.

4.1.6. 5-(2-(4-(Diphenylamino)phenyl)-9,10-bis(2-(triisopropyl-silyl)ethynyl)anthracen-6-yl)thiophene-2-carbaldehyde (6a). A mixture of **4a** (500 mg, 0.6 mmol), (5-(1,3-dioxolan-2-yl)thiophen-2-yl)tributylstannane (517 mg, 1.2 mmol), $PdCl_2(PPh_3)_2$ (20.4 mg, 0.03 mmol) were dissolved in dry DMF, then heated to 90 °C with stirring. After 24 h, the reaction was cooled to room temperature, then quenched by the addition of methanol and saturated $KF_{(aq)}$ (15 mL). The mixture was extracted with CH_2Cl_2 , while the organic layer was dried over anhydrous $MgSO_4$. Evaporation of the solvent gave a crude product. The crude mixture was added Acetic acid/THF/de-ionized water (40/20/10 mL) at 90 °C. After 3 h, the reaction was quenched by adding de-ionized water and brine. To mixture extracted with CH_2Cl_2 , and the organic layer was dried over anhydrous $MgSO_4$ and evaporated under vacuum, which was purified by silica gel column chromatograph eluted by CH_2Cl_2 /hexane (1/4). Red solid of **6a** was obtained in 55% yield (285 mg, 0.3 mmol); mp 165–167 °C; 1H NMR (400 MHz, $CDCl_3$): δ 9.94 (s, 1H), 9.00 (s, 1H), 8.85 (s, 1H), 8.66 (d, 2H, $J=8.9$ Hz), 7.86–7.93 (m, 2H), 7.81 (d, 1H, $J=3.9$ Hz), 7.70 (d, 2H, $J=8.5$ Hz), 7.61 (d, 1H, $J=3.8$ Hz), 7.30 (t, 4H, $J=7.8$ Hz), 7.17–7.20 (m, 6H), 7.0 (t, 2H, $J=7.3$ Hz), 1.2–1.3 (m, 42H); ^{13}C NMR (100 MHz, $CDCl_3$): δ 182.5, 154.0, 147.8, 147.5, 142.8, 139.0, 137.3, 133.9, 133.3, 132.4, 132.1, 131.9, 130.9, 129.3, 128.4, 128.0, 127.8, 126.9, 124.9, 124.6, 123.9, 123.6, 123.1, 119.1, 118.6, 105.9, 105.52, 103.0, 102.8, 18.9, 11.5; MS (FAB, 70 eV): m/z (relative intensity) 892 (($M+H$) $^+$, 100); HRMS calcd for $C_{59}H_{66}NOSSi_2$: 892.4404, found 892.4438.

4.1.7. 5-(2-(4-(Diphenylamino)phenyl)-9,10-dibutylanthracen-6-yl)thiophene-2-carbaldehyde (6b). Compound **6b** was synthesized according to the same procedure as that of **6a**. Light yellow solid of **6b** was obtained in 51% yield; mp 145–147 °C; 1H NMR (400 MHz, $CDCl_3$): δ 9.93 (s, 1H), 8.63 (d, 1H, $J=1.6$ Hz), 8.44 (d, 1H, $J=1.3$ Hz), 8.36 (d, 1H, $J=9.2$ Hz), 8.35 (d, 1H, $J=9.2$ Hz), 7.78–7.82 (m, 2H), 7.76 (dd, 1H, $J=9.3, 1.3$ Hz), 7.67 (d, 2H, $J=8.6$ Hz), 7.58 (d, 1H, $J=3.8$ Hz), 7.30 (t, 4H, $J=7.8$ Hz), 7.22 (d, 2H, $J=8.5$ Hz), 7.18 (d, 4H, $J=7.6$ Hz), 7.06 (t, 2H, $J=7.3$ Hz), 3.60–3.65 (m, 4H), 1.84–1.86 (m, 4H), 1.61–1.66 (m, 4H), 1.03–1.10 (m, 6H); ^{13}C NMR (100 MHz, $CDCl_3$): δ 182.7, 155.0, 147.6, 147.5, 142.2, 137.6, 137.1, 134.9, 134.7, 134.2, 130.4, 129.3, 129.1, 128.9, 128.8, 127.9, 126.5, 125.9, 125.1, 124.6, 124.1, 123.7, 123.2, 123.1, 122.7, 121.9, 33.817, 33.640, 27.8, 23.4, 14.1; MS (FAB, 70 eV): m/z (relative intensity) 643 (M^+ , 100); HRMS calcd for $C_{45}H_{41}NOS$: 643.2908, found 643.2926.

4.1.8. (E)-3-(5-(2-(4-(Diphenylamino)phenyl)-9,10-bis(2-(triiso-propylsilyl)ethynyl)anthracen-6-yl)thiophen-2-yl)-2-cyanoacrylic acid (AN-TIPS). A mixture of **6a** (1.0 g, 1.0 mmol), cyanoacetic acid (128 mg, 1.50 mmol), and ammonium acetate (20 mg, 0.25 mmol) in acetic acid was placed in a three-necked flask under a nitrogen atmosphere and was heated to 90–100 °C with stirring for 12 h. After cooling, the reaction was quenched by adding distilled water, and extracted with CH_2Cl_2 . The organic layer was dried over anhydrous $MgSO_4$ and evaporated under vacuum. The product was purified by silica gel column chromatograph eluted by CH_2Cl_2 /acetic acid (19/1). The dark-red solid was isolated in 61% yield (584 mg, 0.61 mmol). Mp 176–178 °C; IR (KBr) ν_{max} 3404, 2923, 2862, 1688, 1566, 1420 cm^{-1} ; 1H NMR (400 MHz, $DMSO-d_6$): δ 9.02 (d, 1H, $J=1.6$ Hz), 8.91 (d, 1H, $J=1.52$ Hz), 8.71 (d, 2H, $J=9.0$ Hz), 8.39 (s, 1H), 8.04–8.11 (m, 2H), 7.94 (d, 1H, $J=4.0$ Hz), 7.80 (d, 2H, $J=3.6$ Hz), 7.77 (s, 1H), 7.27 (t, 4H, $J=7.8$ Hz), 7.18 (d, 2H, $J=3.2$ Hz), 7.14 (d, 4H, $J=7.8$ Hz), 7.04 (t, 2H, $J=7.4$ Hz) 1.30–1.35 (m, 42H); ^{13}C NMR (100 MHz, $DMSO-d_6$): δ 153.6, 149.3, 148.7, 140.5, 140.1, 134.7, 134.3, 133.4, 133.1, 132.5, 130.3, 129.2, 129.0, 128.8, 128.0, 126.5, 126.3, 125.6, 125.3, 125.2, 124.6, 124.5, 124.2, 120.0, 119.4, 107.1,

106.3, 104.3, 104.0, 67.7, 67.5, 67.3, 67.2, 30.7, 30.4, 30.3, 30.2, 30.1, 25.7, 25.6, 25.4, 25.3, 25.1, 19.6, 19.5, 12.7, 12.6. MS (FAB, 70 eV): m/z (relative intensity) 958 (M^+ , 100); HRMS calcd for $C_{62}H_{66}N_2O_2SSi_2$: 958.4384, found 958.4408.

4.1.9. (E)-3-(5-(2-(4-(Diphenylamino)phenyl)-9,10-dibutyl-anthracen-6-yl)thiophen-2-yl)-2-cyanoacrylic acid (AN-Bu). Compound **AN-Bu** was synthesized according to the same procedure as that of **AN-TIPS**. Dark red solid of **AN-Bu** was obtained in 70% yield; mp 159–161 °C; IR (KBr) ν_{max} 3526, 2955, 2852, 1692, 1683, 1498, 1413, 1315 cm^{-1} ; 1H NMR (400 MHz, $CDCl_3$): δ 8.47 (s, 1H), 8.45 (s, 1H), 8.44 (d, 1H, $J=2.0$ Hz), 8.42 (d, 1H, $J=2.1$ Hz), 8.40 (s, 1H), 7.94 (d, 1H, $J=4.0$ Hz), 7.88 (d, 1H, $J=9.2$ Hz), 7.85 (d, 1H, $J=9.2$ Hz), 7.78 (d, 1H, $J=3.9$ Hz), 7.74 (d, 2H, $J=8.4$ Hz), 7.28 (t, 4H, $J=7.7$ Hz), 7.18 (d, 2H, $J=8.4$ Hz), 7.13 (d, 4H, $J=7.9$ Hz), 7.03 (t, 2H, $J=7.7$ Hz), 3.68–3.76 (m, 4H), 1.81–1.88 (m, 4H), 1.60–1.68 (m, 4H), 1.10 (t, 3H, $J=7.3$ Hz), 1.04 (t, 3H, $J=7.3$ Hz); ^{13}C NMR (100 MHz, $CDCl_3$): δ 164.4, 148.8, 148.7, 146.3, 139.9, 138.2, 136.6, 136.0, 135.9, 135.1, 131.6, 130.6, 130.4, 130.3, 130.2, 130.1, 128.8, 127.5, 127.0, 126.0, 125.7, 125.5, 124.8, 124.1, 123.8, 122.7, 116.9, 34.9, 34.8, 28.6, 28.5, 14.7, 14.6; MS (FAB, 70 eV): m/z (relative intensity) 710 (($M+H$) $^+$, 100); HRMS calcd for $C_{48}H_{43}N_2O_2S$: 710.2967, found 710.2991.

4.2. Fabrication of DSSCs and characterization of DSSCs

The FTO conducting glass (FTO glass, fluorine doped tin oxide over-layer, transmission >90% in the visible, sheet resistance 8 Ω square $^{-1}$), titania-oxide pastes of Ti-Nanoxide T/SP and Ti-Nanoxide R/SP were purchased from Solaronix. A thin film of TiO_2 (16–18 μm thick) was coated on a 0.25 cm^2 FTO glass substrate, while the thickness was measured by Veeco Dektak 150. It was immersed in a THF solution containing 3×10^{-4} M dye sensitizers for at least 12 h, then rinsed with anhydrous acetonitrile and dried. Another piece of FTO with sputtering 100 nm thick Pt was used as a counter electrode. The active area was controlled at a dimension of 0.25 cm^2 by adhering 60 μm thick polyester tape on the Pt electrode. The photocathode was placed on top of the counter electrode and was tightly clipped together to form a cell. Electrolyte was then injected into the seam between two electrodes. Two kinds of electrolytes were used in order to achieve the best result, i.e., system E1 was made of Lil (0.5 M), I_2 (0.05 M), and TBP (4-*tert*-butylpyridine) (0.5 M) in MeCN, and system E2 was composed of 3-dimethylimidazolium iodide (DMII) (1.0 M) and guanidinium thiocyanate (0.1 M), in addition to Lil (0.05 M), I_2 (0.03 M), and TBP (0.5 M) in a mixed solvent of MeCN and valeronitrile (85:15, v/v). Devices made of a commercial dye N719 under the same condition (3×10^{-4} M, Solaronix S.A., Switzerland) was used as a reference.

The cell parameters were obtained under an incident light with intensity 100 mW cm^{-2} measured by a thermopile probe (Oriel 71964), which was generated by a 300 W Xe lamp (Oriel 6258) passing through an AM 1.5 filter (Oriel 81088). The current-voltage parameters of DSSCs were recorded by a potentiostat/galvanostat model CHI650B (CH Instruments, USA). The light intensity was further calibrated by an Oriel reference solar cell (Oriel 91150) and adjusted to be 1.0 sun. The monochromatic quantum efficiency was recorded through a monochromator (Oriel 74100) at short-circuit condition. Electrochemical impedance spectra of DSSCs were recorded by an Impedance/Gain-Phase analyzer (SI 1260, Solartron).

4.3. Theoretical calculation

All organic dyes were optimized by using B3LYP/6-31G* hybrid functional. Geometry optimizations were performed to locate the minima on the potential energy surface, in order to predict the equilibrium structure of a given molecule. For the excited states,

a time-dependent density functional theory (TDDFT) with the B3LYP functional was employed. All analyses were performed under Q-Chem 3.0 software. The frontier orbital plots of HOMO and LUMO were drawn by using Gaussian 03. All calculations were performed using the Gaussian 03 suite of programs.

Acknowledgements

Financial supports from the National Science Council of Taiwan and Academia Sinica are gratefully acknowledged. (NSC 101-2113-M-035-001-MY2) Special thanks to Professor C.-P. Hsu in the Institute of Chemistry, Academia Sinica, for the assistance on Quantum chemistry computations.

Supplementary data

¹H And ¹³C NMR spectra of all compounds, absorption spectra and emission spectra in THF solution, absorption spectra on TiO₂ film, TDDFT calculated orbitals, Mulliken charges, low energy transitions, CV spectra, HOMO/LUMO level, and EIS spectra. Supplementary data related to this article can be found at <http://dx.doi.org/10.1016/j.tet.2013.11.072>

References and notes

- O'Regan, B.; Grätzel, M. *Nature* **1991**, *353*, 737–740.
- Grätzel, M. *Nature* **2003**, *414*, 338–344.
- Nazeeruddin, M. K.; Key, A.; Rodicio, I.; Humphry-Baker, R.; Müller, E.; Liska, P.; Vlachopoulos, N.; Grätzel, M. *J. Am. Chem. Soc.* **1993**, *115*, 6382–6390.
- Nazeeruddin, M. K.; Péchy, P.; Renouard, T.; Zakeeruddin, S. M.; Humphry-Baker, R.; Comte, P.; Liska, P.; Cevey, L.; Costa, E.; Shklover, V.; Spiccia, L.; Deacon, G. B.; Bignozzi, C. A.; Grätzel, M. *J. Am. Chem. Soc.* **2001**, *123*, 1613–1624.
- Wang, Z.-S.; Cui, Y.; Hara, K.; Dan-oh, Y.; Kasada, C.; Shinpo, A. *Adv. Mater.* **2007**, *19*, 1138–1141.
- Hara, K.; Miyamoto, K.; Yoshimoto, A.; Yanagida, M. *J. Phys. Chem. B* **2005**, *109*, 23776–23778.
- Kuang, D.; Uchida, S.; Humphry-Baker, R.; Zakeeruddin, S. M.; Grätzel, M. *Angew. Chem., Int. Ed.* **2008**, *47*, 1923–1927.
- Ehret, A.; Stuhl, L.; Spittler, M. *T. J. Phys. Chem. B* **2001**, *105*, 9960–9965.
- Sayama, K.; Hara, K.; Ohga, Y.; Shinpou, A.; Suga, S.; Arakawa, H. *New J. Chem.* **2001**, *25*, 200–202.
- Sayama, K.; Tsukagoshi, S.; Hara, K.; Ohga, Y.; Shinpou, A.; Abe, Y.; Suga, S.; Arakawa, H. *J. Phys. Chem. B* **2002**, *106*, 1363–1371.
- Yao, Q.-H.; Shan, L.; Li, F.-Y.; Yin, D.-D.; Huang, C.-H. *New J. Chem.* **2003**, *27*, 1277–1283.
- Yao, Q.-H.; Meng, F.-S.; Li, F.-Y.; Tian, H.; Huang, C.-H. *J. Mater. Chem.* **2003**, *13*, 1048–1053.
- Ferrere, S.; Gregg, B. A. *New J. Chem.* **2002**, *26*, 1155–1160.
- Edvinsson, T.; Li, C.; Pschirer, N.; Schöneboom, J.; Eickemeyer, F.; Sens, R.; Boschloo, G.; Herrmann, A.; Müllen, K.; Hagfeldt, A. *J. Phys. Chem. C* **2007**, *111*, 15137–15140.
- Shibano, Y.; Umeyama, T.; Matano, Y.; Imahori, H. *Org. Lett.* **2007**, *9*, 1971–1974.
- Fortage, J.; Séverac, M.; Rassin, C. H.; Pellegrin, Y.; Blart, E.; Odobel, F. *J. Photochem. Photobiol. A* **2008**, *197*, 156–169.
- Imahori, H.; Umeyama, T.; Ito, S. *Acc. Chem. Res.* **2009**, *42*, 1809–1818.
- Ko, S.; Choi, H.; Kang, M.-S.; Hwang, H.; Ji, H.; Kim, J.; Ko, J.; Kang, Y. *J. Mater. Chem.* **2010**, *20*, 2391–2399.
- Lin, L.-Y.; Tsai, C.-H.; Wong, K.-T.; Huang, T.-W.; Hsieh, L.; Liu, S.-H.; Lin, H.-W.; Wu, C.-C.; Chou, S.-H.; Chen, S.-H.; Tsai, A.-I. *J. Org. Chem.* **2010**, *75*, 4778–4785.
- Cho, N.; Choi, H.; Kim, D.; Song, K.; Kang, M. S.; Kang, S. O.; Ko, J. *Tetrahedron* **2009**, *65*, 6236–6243.
- Heredia, D.; Natera, J.; Gervaldo, M.; Otero, L.; Fungo, F.; Lin, C.-Y.; Wong, K.-T. *Org. Lett.* **2010**, *12*, 12–15.
- Zhou, G.; Pschirer, N.; Schöneboom, J. C.; Eickemeyer, F.; Baumgarten, M.; Müllen, K. *Chem. Mater.* **2008**, *20*, 1808–1815.
- Koumura, N.; Wang, Z. S.; Mori, S.; Miyashita, M.; Suzuki, E.; Hara, K. *J. Am. Chem. Soc.* **2006**, *128*, 14256–14257.
- Wang, Z. S.; Koumura, N.; Cui, Y.; Takahashi, M.; Sekiguchi, H.; Mori, S.; Kubo, T.; Furube, A.; Hara, K. *Chem. Mater.* **2008**, *20*, 3993–4003.
- Zhang, X. H.; Wang, Z. S.; Cui, Y.; Koumura, N.; Furube, A.; Hara, K. *J. Phys. Chem. C* **2009**, *113*, 13409–13415.
- Teng, C.; Yang, X.; Yuan, C.; Li, C.; Chen, R.; Tian, H.; Li, S.; Hagfeldt, A.; Sun, L. *Org. Lett.* **2009**, *11*, 5542–5545.
- Chang, Y. J.; Chou, P.-T.; Lin, S.-Y.; Watanabe, M.; Liu, Z.-Q.; Lin, J.-L.; Chen, K.-Y.; Sun, S.-S.; Liu, C.-Y.; Chow, T. J. *Chem.—Asian J.* **2012**, *7*, 572–581.
- Tian, H.; Yang, X.; Chen, R.; Pan, Y.; Li, L.; Hagfeldt, A.; Sun, L. *Chem. Commun.* **2007**, *3741*–3743.
- Kim, S. H.; Kim, H. W.; Sakong, C.; Namgoong, J.; Park, S. W.; Ko, M. J.; Lee, C. H.; Lee, W. I.; Kim, J. P. *Org. Lett.* **2009**, *13*, 5784–55787.
- Wu, W.; Yang, J.; Hua, J.; Tang, J.; Zhang, L.; Long, Y.; Tian, H. *J. Mater. Chem.* **2010**, *20*, 1772–1779.
- Marszalek, M.; Nagane, S.; Ichake, A.; Humphry-Baker, R.; Paul, V.; Zakeeruddin, S. M.; Grätzel, M. *J. Mater. Chem.* **2012**, *22*, 889–894.
- Meyer, T.; Ogermann, D.; Pankrath, A.; Kleinermanns, K.; Müller, T. J. *J. Org. Chem.* **2012**, *77*, 3704–3715.
- Cao, D.; Peng, J.; Hong, Y.; Fang, X.; Wang, L.; Meier, H. *Org. Lett.* **2011**, *13*, 1610–1613.
- Yang, C. J.; Chang, Y. J.; Watanabe, M.; Hon, Y. S.; Chow, T. J. *J. Mater. Chem.* **2012**, *22*, 4040–4049.
- Chang, Y. J.; Chou, P. T.; Lin, Y. Z.; Watanabe, M.; Yang, C. J.; Chin, T. M.; Chow, T. J. *J. Mater. Chem.* **2012**, *22*, 21704–21712.
- Thomas, K. R. J.; Singh, P.; Baheti, A.; Hsu, Y. C.; Ho, K. C.; Lin, J. T. *Dyes Pigm.* **2011**, *91*, 33–43.
- Lin, R. Y. Y.; Yen, Y. S.; Cheng, Y. T.; Lee, C. P.; Hsu, Y. C.; Chou, H. H.; Hsu, C. Y.; Chen, Y. C.; Lin, J. T.; Ho, K. C.; Tsai, C. *Org. Lett.* **2012**, *14*, 3612–3615.
- Lin, Y. D.; Chien, C. T.; Lin, S. Y.; Chang, H. H.; Liu, C. Y.; Chow, T. J. *J. Photochem. Photobiol. A* **2011**, *222*, 192–202.
- Lin, Y. D.; Chow, T. J. *J. Mater. Chem.* **2011**, *21*, 14907–14916.
- Jung, K. H.; Bae, S. Y.; Kim, K. H.; Cho, M. J.; Lee, K.; Kim, Z. H.; Choi, D. H.; Lee, D. H.; Chung, D. S.; Park, C. E. *Chem. Commun.* **2009**, *5290*–5292.
- Hur, J. A.; Bae, S. Y.; Kim, K. H.; Lee, T. W.; Cho, M. J.; Choi, D. H. *Org. Lett.* **2011**, *13*, 1948–1951.
- Miyaura, N.; Suzuki, A. *Chem. Rev.* **1995**, *95*, 2457–2483.
- Stille, J. K. *Angew. Chem., Int. Ed. Engl.* **1986**, *25*, 508–524.
- Knoevenagel, E. *Angew. Chem., Int. Ed. Engl.* **1922**, *35*, 29–30.
- Choi, H.; Lee, J. K.; Song, K.; Kang, S. O.; Ko, J. *Tetrahedron* **2007**, *63*, 3115–3121.
- Chen, R.; Yang, X.; Tian, H.; Wang, X.; Hagfeldt, A.; Sun, L. *Chem. Mater.* **2007**, *19*, 4007–4015.
- Hara, K.; Wang, Z. S.; Sato, T.; Furube, A.; Katoh, R.; Sugihara, H.; Dan-oh, Y.; Kasada, C.; Shinpo, A.; Suga, S. *J. Phys. Chem. B* **2005**, *109*, 15476–15482.
- Hagfeldt, A.; Grätzel, M. *Chem. Rev.* **1995**, *95*, 49–68.
- Hara, K.; Sato, T.; Katoh, R.; Furube, A.; Ohga, Y.; Shinpo, A.; Suga, S.; Sayama, K.; Sugihara, H.; Arakawa, H. *J. Phys. Chem. B* **2003**, *107*, 597–606.
- Shao, Y.; Molnar, L. F.; Jung, Y.; Kussmann, J.; Ochsenfeld, C.; Brown, S. T.; Gilbert, A. T. B.; Slipchenko, L. V.; Levchenko, S. V.; O'Neill, D. P.; DiStasio, R. A., Jr.; Lochan, R. C.; Wang, T.; Beran, G. J. O.; Besley, N. A.; Herbert, J. M.; Lin, C. Y.; Voorhis, T. V.; Chien, S. H.; Sodt, A.; Steele, R. P.; Rassolov, V. A.; Maslen, P. E.; Korambath, P. P.; Adamson, R. D.; Austin, B.; Baker, J.; Byrd, E. F. C.; Dachsel, H.; Doerkens, R. J.; Drew, A.; Dunietz, B. D.; Dutoi, A. D.; Furlani, T. R.; Gwaltney, S. R.; Heyden, A.; Hirata, S.; Hsu, C. –P.; Kedziora, G.; Khalililun, R. Z.; Klunzinger, P.; Lee, A. M.; Lee, M. S.; Liang, W. Z.; Lotan, I.; Nair, N.; Peters, B.; Proynov, E. I.; Pieniazek, P. A.; Rhee, Y. M.; Ritchie, J.; Rosta, E.; Sherrill, C. D.; Simmonett, A. C.; Subotnik, J. E.; Woodcock, H. L., III; Zhang, W.; Bell, A. T.; Chakraborty, A. K. *Phys. Chem. Chem. Phys.* **2006**, *8*, 3172–3191.
- Boschloo, G.; Häggman, L.; Hagfeldt, A. *J. Phys. Chem. B* **2006**, *110*, 13144–13150.
- Ning, Z.; Fu, Y.; Tian, H. *Energy Environ. Sci.* **2010**, *3*, 1170–1181.
- Haque, S. A.; Palomares, E.; Cho, B. M.; Green, A. N. M.; Hirita, N.; Klug, D. R.; Durrant, J. R. *J. Am. Chem. Soc.* **2005**, *127*, 3456–3462.
- Fabregat-Santiago, F.; Bisquert, J.; García-Belmonte, G.; Boschloo, G.; Hagfeldt, A. *Sol. Energy Mater. Sol. Cells* **2005**, *87*, 117–131.
- Wang, Q.; Moser, J.-E.; Grätzel, M. *J. Phys. Chem. B* **2005**, *109*, 14945–14953.
- Hara, K.; Dan-oh, Y.; Kasada, C.; Ohga, Y.; Shinpo, A.; Suga, S.; Sayama, K.; Arakawa, H. *Langmuir* **2004**, *20*, 4205–4210.
- Wang, Z.-S.; Cui, Y.; Dan-oh, Y.; Kasada, C.; Shinpo, A.; Hara, K. *J. Phys. Chem. C* **2007**, *111*, 7224–7230.
- Liu, B.; Zhu, W.; Zhang, Q.; Wu, W.; Xu, M.; Ning, Z.; Xie, Y.; Tian, H. *Chem. Commun.* **2009**, *1766*–1768.
- Shen, P.; Liu, Y.; Huang, X.; Zhao, B.; Xiang, N.; Fei, J.; Liu, L.; Wang, X.; Huang, H.; Tan, S. *Dyes Pigm.* **2009**, *83*, 187–197.
- Tian, H.; Yang, X.; Cong, J.; Chen, R.; Teng, C.; Liu, J.; Hao, Y.; Wang, L.; Sun, L. *Dyes Pigm.* **2010**, *84*, 62–68.
- Tang, J.; Hua, J.; Wu, W.; Li, J.; Jin, Z.; Long, Y.; Tian, H. *Energy Environ. Sci.* **2010**, *3*, 1736–1745.
- Chen, B. S.; Chen, D. Y.; Chen, C. L.; Hsu, C. W.; Hsu, H. C.; Wu, K. L.; Liu, S. H.; Chou, P. T.; Chi, Y. *J. Mater. Chem.* **2011**, *21*, 1937–1945.
- Lee, S. K.; Yang, W. J.; Choi, J. J.; Kim, C. H.; Jeon, S.-J.; Cho, B. R. *Org. Lett.* **2005**, *7*, 323–326.
- Park, J.-H.; Chung, D. S.; Park, J.-W.; Ahn, T.; Kong, H.; Jung, Y. K.; Lee, J.; Yi, M. H.; Park, C. E.; Kwon, S.-K.; Shim, H.-K. *Org. Lett.* **2007**, *9*, 2573–2576.
- Lin, R. Y.-Y.; Lin, H.-W.; Yen, Y.-S.; Chang, C.-H.; Chou, H.-H.; Chen, P.-W.; Hsu, C.-Y.; Chen, Y.-C.; Lin, J. T.; Ho, K.-C. *Energy Environ. Sci.* **2013**, *6*, 2477–2486.
- Teng, C.; Yang, X.; Yang, C.; Li, S.; Cheng, M.; Hagfeldt, A.; Sun, L. *J. Phys. Chem. C* **2010**, *114*, 9101–9110.